ISSN 2090-3359 (Print)
ISSN 2090-3367 (Online)

Advances in Decision Sciences

Volume 26
Special Issue in Honour of Michael McAleer
2022 - 2023

Michael McAleer (Editor-in-Chief)
Chia-Lin Chang (Senior Co-Editor-in-Chief)
Alan Wing-Keung Wong (Senior Co-Editor-in-Chief and Managing Editor)
Aviral Kumar Tiwari (Co-Editor-in-Chief)
Montgomery Van Wart (Associate Editor-in-Chief)
Vincent Shin-Hung Pan (Managing Editor)

Published by Asia University, Taiwan

Analysis of Electrically Couple SRR EBG Structure for Sub 6 GHz Wireless Applications

Iqbal Jebril
Department of Mathematics, Al-Zaytoonah University of Jordan, Amman 11942
email: Jordani.jebril@zuj.edu.jo

P. Dhanaraj
RF Designer, Special Coverage Division, Net Coverage Solutions Limited,
Camberley, United Kingdom,
email:dhanswt2@gmail.com

Ghaida Muttashar Abdulsahib
Department of Computer Engineering,University of Technology, Baghdad, Iraq
e-mail: ghaida.m.abdulsaheb@uotechnology.edu.iq

SatheeshKumar Palanisamy*
Department of ECE, Coimbatore Institute of Technology, Coimbatore, Tamilnadu, India
**Corresponding Author*: e-mail: satheeshkumar.p@cit.edu.in

T.Prabhu
Department of Electronics and Communication Engineering, Presidency University
Bengaluru, Karnataka, India,
e-mail:prabhu@presidencyuniversity.in

Osamah Ibrahim Khalaf
Department of Solar ,Al-Nahrain Research Center for Renewable Energy,
Al-Nahrain University, Jadriya, Baghdad, Iraq
e-mail: usama81818@nahrainuniv.edu.iq

Received: June 18, 2023; First Revision: June 25, 2023;

Last Revision: June 30, 2023; Accepted: June 30, 2023;

Published: July 1, 2023

Abstract

Purpose – For 5G wireless communication at frequencies below 6 GHz, this research describes an electromagnetic bandgap (EBG) structure based on an electrically coupled split-ring resonator (ECSRR). To create the EBG, the ECSRR is embedded within a structure similar to an interdigital capacitor.

Design/methodology/approach – The proposed EBG design is composed of an electrically coupled structure that resembles an interdigital capacitor and a structure built of split-ring resonators. The proposed EBG structure was printed on a FR4 substrate that had a 4.4, 1.6 millimeters thickness, and a tan =0.025. An interdigital capacitor-like structure is connected to the inner split-rings, and the top layer consists of two sets of split-ring resonators that are electrically connected. A wire-like structure is printed on the substrate's bottom layer.

Findings – The suggested ECSRR EBG structure has a reflection phase bandwidth of 2.65 GHz between 3.5 and 6.15 GHz, and also a bandgap property bandwidth of 2.9 GHz between 3.3 and 6.2 GHz. Without an EBG structure, the CPW-fed microstrip quarter wave monopole antenna has a gain(maximum) of 2.574 dBi at 4.15 GHz and a bandwidth of 4.6 GHz between 3.4 and 8 GHz. Gain(maximum)of 8.785 dBi is achieved at 4.15 GHz when the ECSRR EBG structure is combined with a CPW-fed microstrip quarter wave monopole antenna .

Originality– The suggested ECSRR EBG structure is merged with a two-element ECSRR bow-tie antenna to verify its bandgap property. By inserting the ECSRR EBG structure's 2x4 array in between the two elements of the bow-tie antenna, we can decrease their mutual coupling. Maximum isolation is achieved at 4.9 GHz, with mutual coupling below -32 dB over the whole operational frequency range. Decision science enables antenna designers to analyze, optimize, and track the performance of the antenna characteristics. The following are some of the potential benefits of the proposed study:

It is argued that statistical and regression properties can be used to create a powerful tool for feature extraction. To better understand how antenna design choices affect antenna performance, we compare different regression models. To accurately calculate the S parameters from the relevant UWB antenna dimensions, a random forest classifier that has been optimized for this task has been developed.

***Keywords*:** ECSRR; Split ring resonator; Sub 6 GHz; Bowtie antenna; Metamaterial; Beam tilting; Isolation; MIMO; EBG;

JEL classification: C02, C14, C32, C38, C53

1. Introduction

This paper presents an electrically coupled split-ring resonator (ECSRR) Electromagnetic Bandgap(EBG) structure for sub-6 GHz 5G wireless communication. The Electromagnetic Bandgap(EBG) structure is designed by embedding an inter-digital capacitor-like structure with the ECSRR. The proposed ECSRR EBG structure achieves a 2.65 GHz reflection phase bandwidth of 3.5 GHz to 6.15 GHz and a 2.9 GHz bandgap property bandwidth from 3.3 GHz to 6.2 GHz (Batiha et al., 2022; Yasumoto, 2018). The CPW-fed microstrip quarter wave monopole antenna without EBG structure achieves a broader bandwidth of 4.6 GHz from 3.4 GHz to 8 GHz and a gain(maximum)of 2.574 dBi at 4.15 GHz. The integration of the ECSRR EBG structure with a CPW-fed microstrip quarter wave monopole antenna succeeds in a (maximum) gain of 8.785 dBi at 4.15 GHz with a gain enhancement of 6.2 dBi (Lei et al., 2021; Elmezughi et al., 2009). To validate the bandgap property of the recommended ECSRR EBG structure, it is proposed to integrate a 2-element ECSRR bow-tie antenna. The existence of mutual coupling amid the two-element ECSRR bow-tie antenna is reduced by placing the 2x4 array of ECSRR Electromagnetic Bandgap structure in between them (Yang et al., 2013; Leger et al., 2005). The existence of mutual coupling in the operating band of frequency is less than -32 dB, and the maximum isolation of 66 dB at 4.9 GHz.

Multiple antenna systems have made use of EBG structures to improve their mutual coupling (Yang et al., 2003; Ghosh et al., 2014; Yang et al., 2017; Yang et al., 2017; Qamar et al., 2016; Liu et al., 2019). There are a variety of EBG architectures described and discussed (Radisic et al., 1998; Xue et al., 2023; Sharma et al., 2001; Xue et al., 2023; Rifaee et al., 2022; Peng et al., 2010; Mu'Ath et al., 2014; Xue et al., 2023; Tan et al., 2019). The surface current between 4.61 and 5.22 GHz is suppressed by this layout. The extremely narrow stopband of the spiral electromagnetic bandgap structure proposed by Rifaee et al. (2022) is demonstrated. In Peng et al. (2010), a multiband EBG structure is introduced by incorporating a complementary split-ring resonator into a mushroom-shaped EBG. For better isolation between sub-6 GHz quarter-wave monopole antennas based on meander lines, Tan et al. (2019) presented a dual-band split EBG structure. In(Hei et al., 2021; Prabhu et al., 2021; Dash et al., 2023; Prabhu et al., 2021), we see the many ways that EBG structures can be used to boost gain. Periodic traditional square patches resembling mushrooms are joined together in the EBG via a bridge-like structure. In this study, the design and analysis of the reflection property and bandgap of an innovative electrically coupled SRR (ECSRR)-based EBG structure is proposed. Various antenna embeddings are used to examine the potential uses of the proposed ECB structure (Jiang et al., 2019; Rafiei et al., 2018).

2. Design of Electrically Coupled EBG Structure

The proposed EBG design is composed of an electrically coupled structure that resembles an interdigital capacitor and a structure built of split-ring resonators (Suganya et al., 2023; Xue et al., 2023; Kandasamy et al., 2022). The proposed EBG structure was printed on a FR4 substrate that

had a ε_r = 4.4, 1.6 millimeters thickness, and a tan δ =0.025(Alzyadat et al., 2022; Satheesh et al., 2021). An interdigital capacitor-like structure is connected to the inner split rings, and the top layer consists of two sets of split-ring resonators that are electrically connected. A wire-like structure is printed on the substrate's bottom layer. The novel electromagnetic bandgap structure's unit cell structure is shown in Figure 1.

Ring width and ring gap are both set at 0.2 mm in the circular electrically linked SRR EBG unit cell. In Table 1, you can see the exact measurements of the SSR EBG unit with electrical coupling (Abdulsahibet al., 2021; Dhanaraj et al., 2020; Palanisamy et al., 2022). The substrate's wire-like structure is 8.7 mm in length and 0.3 mm in breadth. Each split ring has a different outer diameter, with the larger one measuring 1.8 mm and the smaller one measuring 1.4 mm. The inner split rings are where the capacitor-like interdigital structure is connected (Palanisamy et al., 2022).

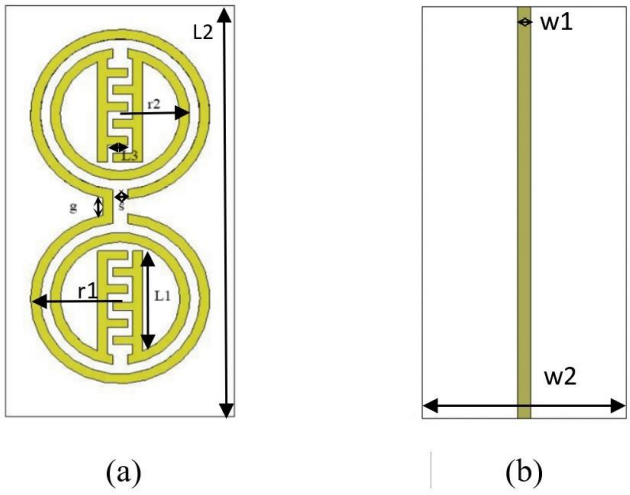

Figure. 1. Structure of proposed EBG unit cell (a) Top Layer (b) Bottom Layer

Table 1. Electrically Coupled SRR EBG Dimensions

Parameter	Dimension in mm
r_1	1.8
r_2	1.4
L_1	2.2
L_2	0.4
L_3	8.7
g	0.4
s	0.3
w_1	0.3
w_2	4.6

Adding a structure similar to an interdigital capacitor boosts the capacitance of the unit cell. The inductance is set by the wire-like structure at the base of the FR4 substrate. The interdigital capacitor-like structure provides flexibility in tuning the bandgap frequency bands. The centre frequency (eq.1) of the EBG structure is

$$f_o = \frac{1}{2\pi\sqrt{LC}} \tag{1}$$

2.1 Reflection Phase of ECSRR EBG unit cell

The proposed electrically Coupled SRR EBG unit cell has been modelled in the CST for simulation purposes. The YZ plane employs the PMC boundary condition (Perfect Magnetic Conductor), while the XZ plane uses the PEC boundary condition (Khalaf et al., 2022; Palanisamy et al., 2021; Palanisamy et al., 2021). Waveguide ports in the Z direction are used to feed the plane wave input, allowing the reflection property of the electrically connected SRR EBG unit cell to be measured. Reflection analysis of artificial magnetic conductors is crucial for deducing their in-phase reflection properties.

For the proposed electrically connected EBG unit cell, Figure 2 displays the reflection phase obtained by numerical simulation. Reflection bandwidth is most useful between -90 and +90 degrees on either side of the resonance frequency. When the angle of reflection is between 0 and 90 degrees, the reflected plane waves have the same phase as the incident wave (Kumar et al., 2021; Dey et al., 2021; Palanisamy et al., 2022). To achieve the necessary bandwidth and the zero reflection phase frequency, a structure similar to interdigital capacitors is optimised. To achieve the desired performance, the interdigital capacitor-like structure's arm count and arm spacing are modified.

From 3.5 GHz to 6.15 GHz, the suggested structure achieves a 2.65 GHz in-phase reflection bandwidth.

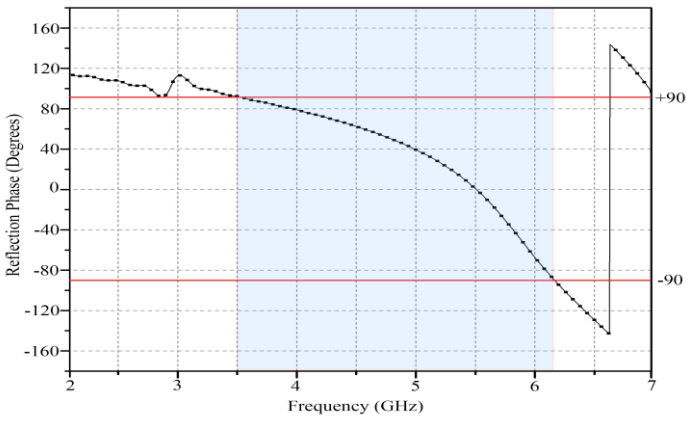

Figure 2. Reflection Phase of electrically coupled SRR EBG

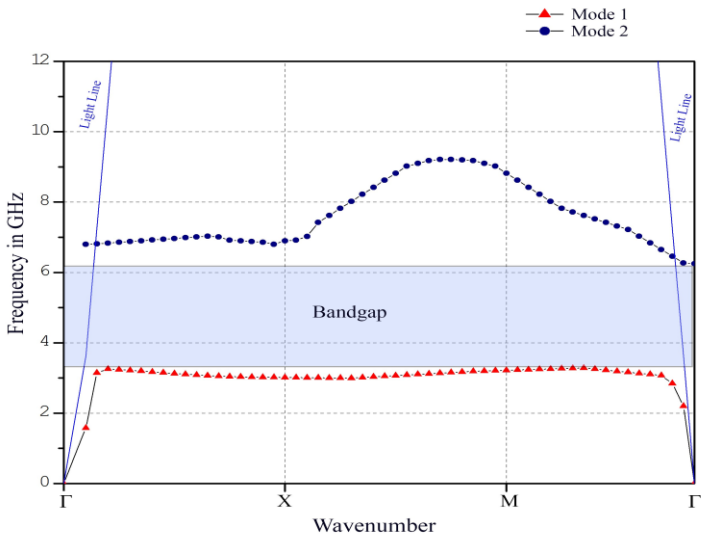

Figure 3. Dispersion diagram of ECSRR EBG

At 5.5 GHz, there is no phase reflection with the suggested architecture. This design outperforms the previously developed ECSRR metamaterial unit cell in terms of bandwidth.

2.2 Dispersion Diagram of ECSRR EBG unit cell

Both the x and y axes of the unit cell are subjected to periodic boundary conditions. The CST microwave full-wave simulation software's Eigenmode solver was used to simulate the suggested design. Sweep the phase from (Γ to X) then to (X to M), and (M to Γ) with a step size of 10 degrees to generate the dispersion chart for the proposed ECSRR EBG structure. The first two modes had their 2D dispersion diagrams computed. The first series of computations involves switching the phase in the x-axis from 0 to 180 degrees while keeping it at 0 in the y-axis (Prabhu et al., 2021; Kumar et al., 2021). The phase in the y-axis is adjusted from 0 to 180^0, while the phase in the x-axis is held constant, to model the second series of calculations from X to M. Phase is altered in both the x and y axes concurrently from 0 to 180 degrees to model the third set of M computations. In addition, x and y continue to have the same phase values (Kumar et al., 2012). All three sets of numbers are combined to produce the dispersion diagram of the ECSRR-EBG periodic structure. A bandgap of 2.9 GHz is attained with the suggested electrically connected SRR EBG periodic arrangement. The frequency gap here is between 3.3 and 6.2 GHz.

3 CPW Fed Microstrip Quarter Wave Monopole Antenna

3.1 CPW-fed microstrip quarter wave monopole antenna design

The microstrip quarter wave monopole antenna with coplanar waveguide feed works effectively between the frequencies of 3.5 GHz and 6.15 GHz. In order to analyse the suitability of the proposed electrically coupled SRR EBG structure, the width of the square patch can be calculated by equation (2).

$$Width = \frac{c}{2f_o\sqrt{\frac{\epsilon_r+1}{2}}} \tag{2}$$

where, fo – Resonate frequency, c- speed of light, and ε_r - dielectric constant of the substrate.
In Figure 4, the CPW microstrip quarter wave monopole antenna design is presented. The square patch microstrip quarter wave monopole antenna is fed by a CPW designed over the top layer of the FR4 dielectric substrate. Table 2 displays the dimensions of the CPW-fed antenna. The monopole microstrip antenna has an omnidirectional radiation pattern. Its compact design measures 30mm x 30mm in total. The dimensions of the square radiation patch and the CPW fed line are optimized to achieve the necessary impedance bandwidth of 3.5 GHz to 6 .15 GHz.

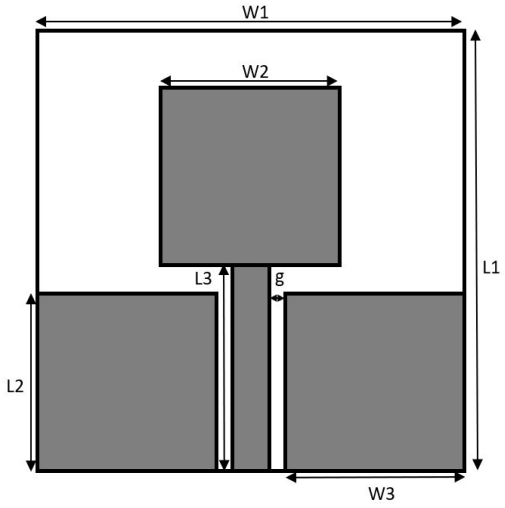

Figure 4. CPW fed microstrip quarter wave monopole antenna

Table 2. Dimensions of CPW Fed Microstrip Quarter Wave Monopole Antenna

Parameter	Dimension in mm
W1	30
W2	13
W3	13.2

L1	30
L2	11.2
L3	14
g	0.3

3.2 Simulation of CPW fed microstrip quarter wave monopole antenna

Figure 5 displays the simulated scattering parameter S_{11} of the proposed CPW-fed microstrip quarter-wave monopole antenna, where the dimensions of the square patch width (W_2) and length of the CPW-fed (L_2) were altered to enhance the impedance matching bandwidth. Various values of W_2 and L_2 were tested.

Based on the simulated result, it appears that widening the square patch leads to a shift in impedance bandwidth towards the lower frequency band (Suganyadevi et al., 2022; Kumar et al., 2021). After conducting a parametric study, it has been determined that the dimensions of L_2 = 13 mm and W_2 = 14 mm provide the necessary maximum impedance matching bandwidth. This design achieves broad bandwidth from 3.4 GHz – 8 GHz. The gain of the CPW-fed microstrip quarter wave monopole antenna is increased by placing the ECSRR EBG periodic structure directly below it. The gain of a CPW-fed microstrip quarter wave monopole antenna can be increased by employing the in-phase reflection artificial magnetic conductor property of ECSRR EBG structures.

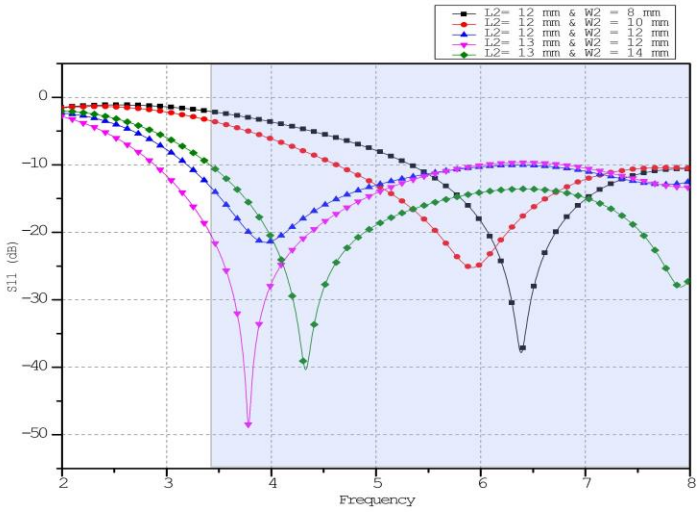

Figure. 5. S-parameter(simulated) of CPW-fed microstrip quarter wave monopole antenna

The schematic for the CPW-fed microstrip quarter wave monopole antenna is shown to describe ECSRR EBG periodic structure at a distance "d." Figure 6 displays a CPW-fed microstrip quarter-wave monopole antenna with an ECSRR and EBG periodic structure. 8 x 4 ECSRR EBG periodic structure below CPW-fed quarter-wave monopole antenna A CST Microwave Studio parametric

analysis changed the antenna-ECSRR EBG periodic structure distance. Figure 7 shows the gain of the ECSRR EBG periodic structure-fed CPW-fed microstrip quarter wave monopole antenna with different spacing "d.". The ECSRR EBG periodic structure's in-phase reflection boosted a CPW-fed microstrip quarter-wave monopole antenna's gain. Simulations show that a 4mm separation improves antenna gain. When placed over the ECSRR EBG periodic structure, the antenna gains 6.07 dBi at 4.5 GHz, according to simulations. The recommended antenna gains 7.4 dBi at 6 GHz, 7.5 at 5.5 GHz, and 5.6 at 3.5 GHz. The ECSRR EBG structure increases the gain of the CPW-fed microstrip quarter-wave monopole antenna from 3.5 GHz to 6 GHz.

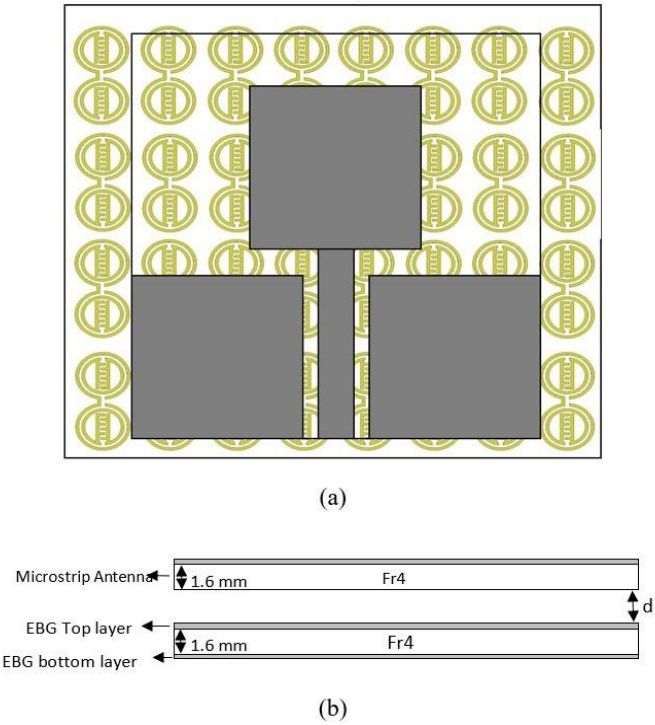

Figure. 6. CPW-fed antenna with ECSRR EBG periodic structure (a) Top view (b) side view

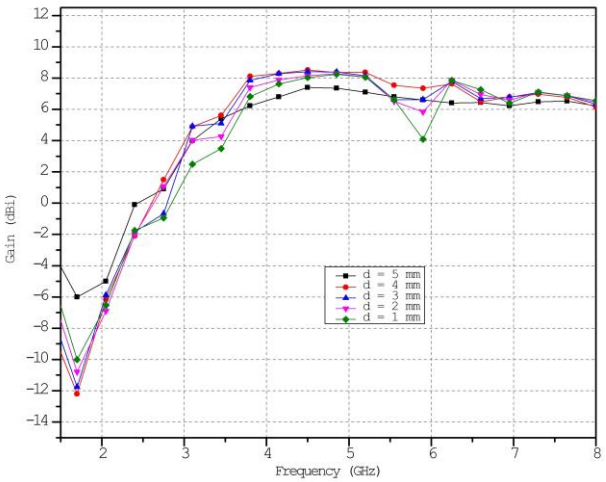

Figure. 7. Simulated gain of the CPW-fed microstrip quarter wave monopole antenna with different 'd' values.

3.4 Experimental results of microstrip quarter wave monopole antenna with ECSRR EBG structure

The real-time measurements have been done in an anechoic chamber and the prototype monopole microstrip patch antenna using the ECSRR EBG reflector are shown in Figures 8 and 9, respectively. The scattering parameter S_{11} of the 4 mm-spaced CPW-fed microstrip quarter wave monopole antenna is shown in Figure 10 along with the corresponding observed value. The antenna accomplishes an excellent impedance-matching bandwidth of 2.6 GHz to 8 GHz. Figure 11 depicts the measured two-dimensional radiation pattern across the operational frequency. The omnidirectional pattern of the antenna is converted into a directional radiation pattern by ECSRR EBG. The gain of a CPW-fed monopole microstrip antenna, both experimentally and numerically, with and without an ECSRR EBG reflector is comparatively analyzed. With a peak gain of 8.785 dBi at 4.15 GHz, this antenna design delivers remarkable performance. The antenna achieves a gain(maximum) 7.5dBi across its entire usable frequency range. The antenna's performance is greatly aided by integrating with the ECSRR EBG structure, which raises the antenna's gain by 6.2 dBi at 4.15 GHz.

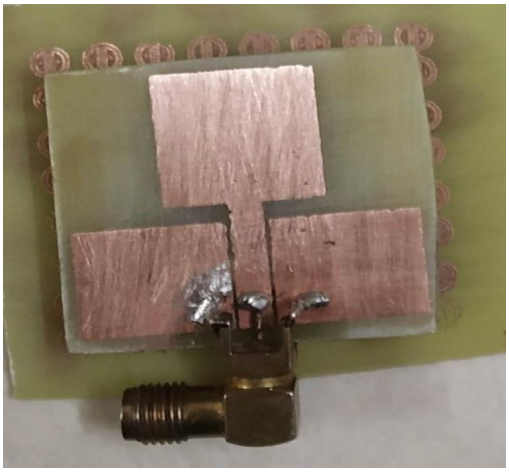

Figure. 8. Prototype model of CPW fed microstrip quarter wave monopole antenna

Figure. 9. Radiation pattern measurement of CPW fed quarter wave monopole antenna with ECSRR EBG reflector in Anechoic chamber

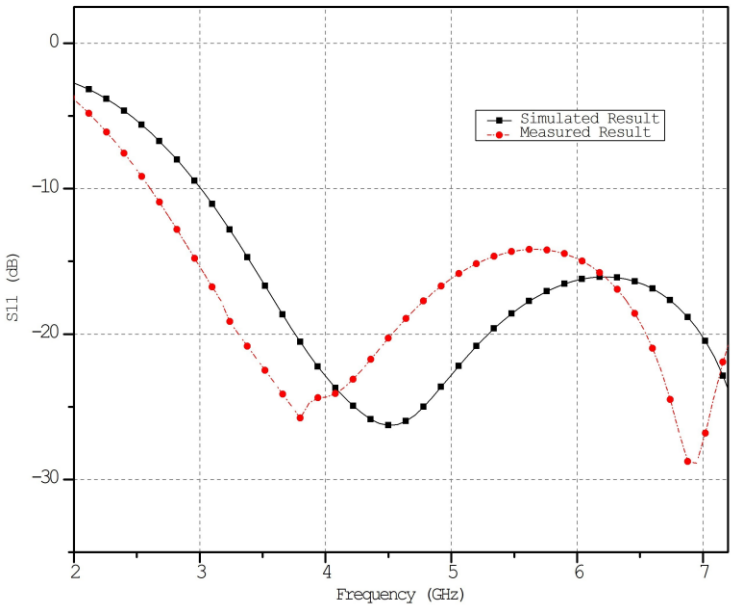

Figure. 10. Comparative analysis of Simulated and measured return loss of CPW fed microstrip antenna with ECSRR EBG periodic structure

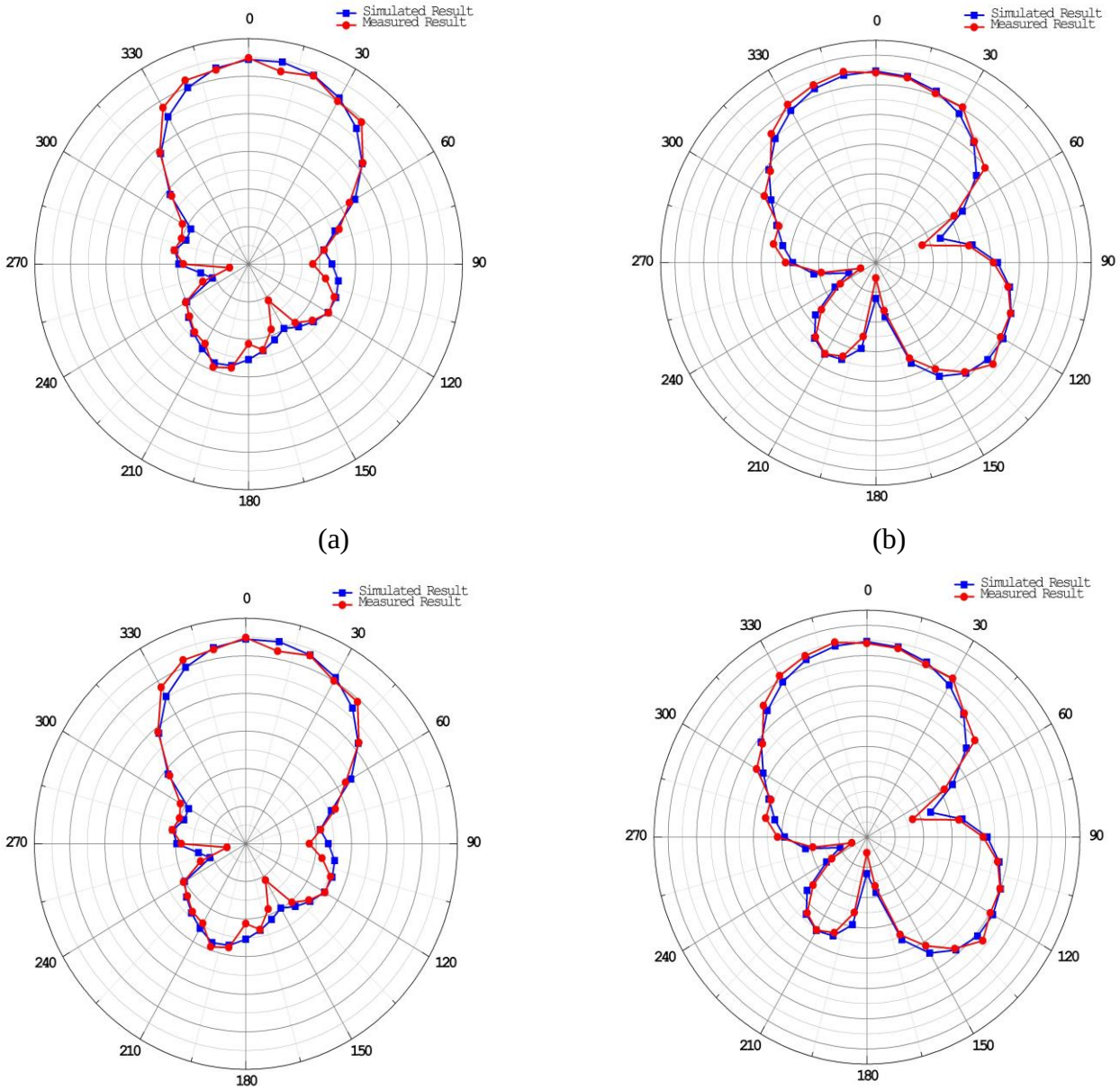

Figure. 11. 2-D Radiation pattern of CPW fed quarter wave monopole antenna with ECSRR EBG structure. (a) 3.5 GHz. (b) 4.45 GHz. (c) 5.45 GHz. (d) 6.15 GHz.

4.2 Simulation of ECSRR bow-tie antenna

The ECSRR bow-tie antenna is microstrip fed, and the wide ground plan is used in the substrate's bottom layer. As a primary component of the bow tie, the ECSRR metamaterial unit cell structure is implemented. The first component has a matching impedance bandwidth of roughly 5.5 GHz. The enhanced bandwidth of 4 GHz to 6 GHz is attained by optimising the second arm length and the size of the ECSRR structure. The ECSRR bow-tie antenna has overall dimensions of 28 mm by 21 mm.

Figure 12 depicts the simulated gain of the ECSRR bow-tie antenna. The gain(maximum) of the simulated ECSRR bow-tie antenna is 4.8 dBi at 4.7 GHz. At 4 GHz, the antenna gains 2.9 dBi; at 5 GHz, it adds 4.7 dBi; at 5.5 GHz, it gains 4.35 dBi; and at 6 GHz, it gains 4 dBi. Across its operational frequency range, the antenna provides a gain of 2.9 dBi at 4 GHz, 4.7 dBi at 5 GHz, 4.35 dBi at 5.5 GHz, and 4 dBi at 6 GHz. The antenna measures 28 x 21 x 1.6 mm in size. The antenna's directed emission pattern and small size are both results of its clever design.

4.3 Gain improvement of ECSRR bow-tie antenna using ECSRR metamaterial unit

The gain of the ECSRR bow-tie antenna is enhanced by the triangular ECSRR metamaterial as described in Xue et al. (2023) is used.

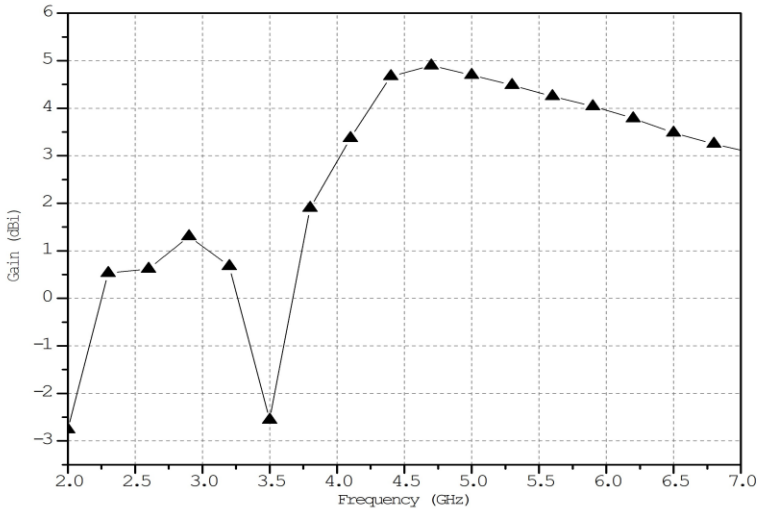

Figure. 12. Simulated gain of the ECSRR bow-tie antenna

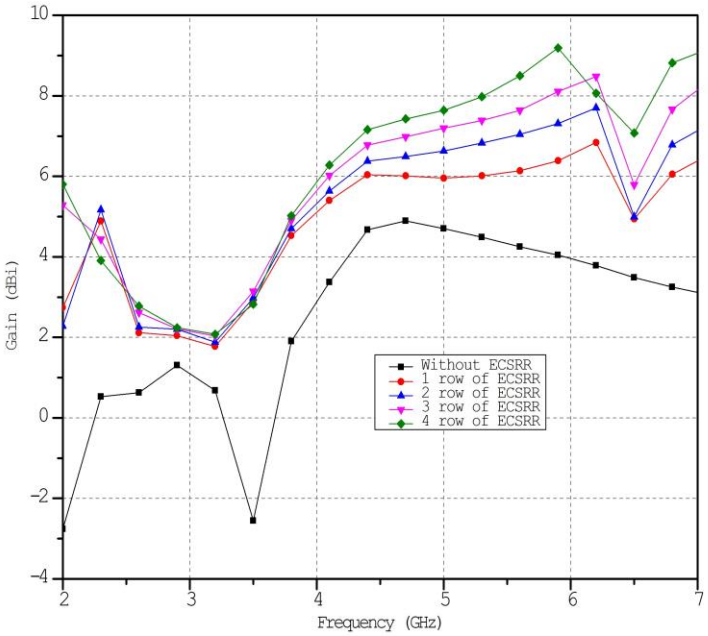

Figure. 13. Simulated gain of ECSRR bow-tie antenna with and without ECSRR metamaterial unit cells

The ECSRR Bowtie antenna and the ECSRR metamaterial unit cells, both in the shape of a triangle, are printed on a FR4 substrate. On the top of the dielectric substrate, the split rings take the form of triangles, while the strip taking the form of a wire is printed there. This concept proposes using an ECSRR bow-tie antenna, which radiates in end-fire array radiation.

Gain in the end-fire direction of an ECSRR bow-tie antenna has been improved by including triangle-shaped ECSRR periodical metamaterial unit cells. A 3x4 array of metamaterial unit cells in the shape of a triangle is included in the ECSRR Bowtie antenna. Three triangle-shaped unit cells are required to provide sufficient coverage along the antenna's length in the end-fire direction.

As a result, the number of cells per unit in the column is set at 3. Analysed the effect of altering the number of rows in the ECSRR metamaterial's unit cell array through parametric research. Figure 13 shows the calculated improvement with and without the ECSRR unit cell. The antenna itself is 28 mm x 49 mm in size. The proposed antenna achieves a gain(maximum)of 9.2 dBi, as seen in the simulation results. The gain of the antenna has been increased by 5.14 dBi at 5.9 GHz thanks to the usage of ECSRR metamaterial unit cells. A 3x4 array of metamaterial unit cells has been shown to exhibit this enhancement. The analysis shows that when the antenna's frequency range expands, its gain also does so.

At 4 GHz, the gain is 6 dBi, while at 5GHz, it goes up to 7.3 dBi. The gain continues to rise to 8.4 dBi at 5.45 GHz and 8.9 dBi at 6.15 GHz. Based on the research, the triangle-shaped ECSRR

metamaterial structure has been proven to elevate the gain of the bowtie antenna within the frequency range of 4GHz to 6GHz.

5. Conclusion

The feasibility of the ECSRR EBG framework is investigated. Integrating the ECSRR EBG structure with a CPW-fed microstrip quarter wave monopole antenna operating in the 3.5–6.15 GHz frequency band demonstrates the EBG structure's ability to improve gain in this setting. The CPW-fed quarter wave monopole antenna's overall gain was improved when an ECSRR bandgap structure was integrated with it for use in the 3.5 GHz to 6.15 GHz range. At 4.15 GHz, it was able to boost gain by 6.2 dBi while maintaining a highly directed emission pattern. The ECSRR EBG structure is combined with the ECSRR bow-tie antenna, which consists of two elements, to study its potential use in reducing mutual coupling. Gain improvements of up to 5.2 dBi at 5.9 GHz and a peak gain of 9.2 dBi are possible because of the incorporation of the ECSRR metamaterial periodic structure into the bow-tie antenna. This frequency range covers 4 to 6 GHz. The mutual coupling and ECC in the 4–6 GHz frequency region were drastically decreased because of the combination of the ECSRR EBG structure and the ECSRR bow-tie antenna, which consists of only two elements. It was able to achieve an isolation of 66 dB at 4.9 GHz and a mutual coupling of less than -32 dB across its entire operating frequency range. Academics and practitioners could extend our paper by using some advanced tools, see, for example, Bai, et al. (2009, 2010), Tiku, et al. (2000), and Li, et al. (2022). Academics and practitioners could also employ the approach used in our paper to examine important issues in other areas, for example, decision sciences, see, for example, Alghalith and Wong (2022), Pham, et al. (2022) and Ravinagarajan and Sophia (2022), economics and finance, see, for example, Maydybura, et al. (2022), Wong, et al. (2022), Obrimah and Wong (2022), etc.

References

Abdulsahib, G. M., & Khalaf, O. I. (2021). An Improved Cross-Layer Proactive Congestion in Wireless Networks. *International Journal of Advances in Soft Computing & Its Applications*, *13*(1).

Alghalith, M., & W.K. Wong. (2022). Option Pricing Under an Abnormal Economy: using the Square Root of the Brownian Motion. *Advances in Decision Sciences* 26: 1-14.

Alzyadat, W., Muhairat, M., Alhroob, A., & Rawashdeh, T. (2022). A Recruitment Big Data Approach to interplay of the Target Drugs. *International Journal of Advances in Soft Computing & Its Applications*, *14*(1).

Bai, Z., Liu, H., & Wong, W. K. (2009). Enhancement of the applicability of Markowitz's portfolio optimization by utilizing random matrix theory. *Mathematical Finance: An International Journal of Mathematics, Statistics and Financial Economics*, *19*(4), 639-667.

Bai, Z., Wong, W. K., & Zhang, B. (2010). Multivariate linear and nonlinear causality tests. *Mathematics and Computers in simulation*, 81(1), 5-17.

Batiha, I. M., Njadat, S. A., Batyha, R. M., Zraiqat, A., Dababneh, A., & Momani, S. (2022). Design fractional-order PID controllers for single-joint robot arm model. *Int. J. Advance Soft Compu. Appl*, *14*(2).

Dash, S., Parida, P., Sahu, G., & Khalaf, O. I. (2023). Artificial Intelligence Models for Blockchain-Based Intelligent Networks Systems: Concepts, Methodologies, Tools, and Applications. In *Handbook of Research on Quantum Computing for Smart Environments* (pp. 343-363). IGI Global. https://doi.org/10.4018/978-1-6684-6697-1.ch019.

Dey, S., Dey, S., & Koul, S. K. (2021). Isolation improvement of MIMO antenna using novel EBG and hair-pin shaped DGS at 5G millimeter wave band. *IEEE Access*, *9*, 162820-162834.

Dhanaraj, P., & Uma Maheswari, S. (2020). Performance analysis of electrically coupled SRR bowtie antenna for wireless broadband communications. *Wireless Networks*, *26*(7), 5271-5283.

Elmezughi, A. S., Rowe, W. S. T., & Waterhouse, R. B. (2009). Edge-fed cavity backed patch antennas and arrays. *IET microwaves, antennas & propagation*, *3*(4), 614-620. doi: 10.1049/iet-map.2008.0172.

Ghosh, S., Tran, T. N., & Le-Ngoc, T. (2014). Dual-layer EBG-based miniaturized multi-element antenna for MIMO systems. *IEEE Transactions on Antennas and Propagation*, *62*(8), 3985-3997. doi: 10.1109/TAP.2014.2323410.

Hei, Y., Wang, M., Wu, W., & Wu, Y. (2021). A Fabry-Perot Cavity Antenna With Non-Uniform Superstrate and EBG Ground for High Gain and High Aperture Efficiency. *IEEE Access*, *9*, 101239-101245.

Jiang, H., Si, L. M., Hu, W., & Lv, X. (2019). A symmetrical dual-beam bowtie antenna with gain enhancement using metamaterial for 5G MIMO applications. *IEEE Photonics Journal*, *11*(1), 1-9.

Kandasamy, A., Rengarasu, S., Kitti Burri, P., Palanisamy, S., Kavin Kumar, K., Baladhandapani, A. D., & Alemayehu Mamo, S. (2022). Defected Circular-Cross Stub Copper Metal Printed

Pentaband Antenna. *Advances in Materials Science and Engineering*, 2022. https://doi.org/10.1155/2022/6009092.

Khalaf, O. I., & Abdulsahib, G. M. (2020). Energy efficient routing and reliable data transmission protocol in WSN. *Int. J. Advance Soft Compu. Appl*, *12*(3), 45-53.

Kumar, P. S., & Valarmathy, S. (2012, March). Development of a novel algorithm for SVMBDT fingerprint classifier based on clustering approach. In *IEEE-International Conference On Advances In Engineering, Science And Management (ICAESM-2012)* (pp. 256-261). IEEE.

Kumar, P. S., Boopathy, S., Dhanasekaran, S., & Anand, K. G. (2021, October). Optimization of multi-band antenna for wireless communication systems using genetic algorithm. In *2021 International Conference on Advancements in Electrical, Electronics, Communication, Computing and Automation (ICAECA)* (pp. 1-6). IEEE. doi: 10.1109/ICAECA52838.2021.9675686.

Kumar, P. S., Chitra, P., & Sneha, S. (2021). Design of improved quadruple-mode bandpass filter using cavity resonator for 5G mid-band applications. *Future Trends in 5G and G*, *6*, 219-234.

Kumar, S., & Balakumaran, T. (2021). Modeling and simulation of dual layered U-slot multiband microstrip patch antenna for wireless applications. *Nanoscale Reports*, *4*(1), 15-18. https://doi.org/10.26524/nr.4.3.

Leger, L., Monediere, T., & Jecko, B. (2005). Enhancement of gain and radiation bandwidth for a planar 1-D EBG antenna. *IEEE Microwave and Wireless Components Letters*, *15*(9), 573-575. doi: 10.1109/LMWC.2005.855373.

Lei, W., Soong, A. C., Jianghua, L., Yong, W., Classon, B., Xiao, W., ... & Saboorian, T. (2020). 5G Fundamental Air Interface Design. *5G System Design: An End to End Perspective*, 35-225. https://doi.org/10.1007/978-3-030-73703-0_3

Li, Z., Jiang, H., Chen, Z., & Wong, W. K. (2022). A mental account-based portfolio selection model with an application for data with smaller dimensions. *Computers & Operations Research*, *144*, 105801.

Liu, Y., Yang, X., Jia, Y., & Guo, Y. J. (2019). A low correlation and mutual coupling MIMO antenna. *IEEE Access*, *7*, 127384-127392.

Maydybura, A., Gohar, R., Salman, A., Wong, W. K., & Chang, B. H. (2022). The Asymmetric Effect of the Extreme Changes in the Economic Policy Uncertainty on the Exchange Rates: Evidence from Emerging Seven Countries. *Annals of Financial Economics*, 2250031.

Mu'Ath, J., Denidni, T. A., & Sebak, A. R. (2014). Millimeter-wave compact EBG structure for mutual coupling reduction applications. *IEEE Transactions on Antennas and Propagation*, *63*(2), 823-828.

Obrimah, O. A., & Wong, W. K. (2022). Modeling of stock returns in continuous vis-á-vis discrete time is equivalent, respectively, to the conditioning of stock returns on a random walk process for trade imbalances vis-á-vis a random walk process for evolution of information. *Annals of Financial Economics*, *17*(02), 2250010.

Palanisamy, S. (2022). Predictive analytics with data visualization. *Journal of Ubiquitous Computing and Communication Technologies*, *4*(2), 75-96. doi:10.36548/jucct.2022.2.003.

Palanisamy, S., & Thangaraju, B. (2022). Design and analysis of clover leaf-shaped fractal antenna integrated with stepped impedance resonator for wireless applications. *International Journal of Communication Systems*, *35*(11), e5184.

Palanisamy, S., Hajjej, F., Khalaf, O. I., & Abdulsahib, G. M. (2022). Discrete Fourier Transform with Denoise Model Based Least Square Wiener Channel Estimator for Channel Estimation in MIMO-OFDM. *Entropy*, *24*(11), 1601. https:// doi.org/10.3390/e24111601.

Palanisamy, S., Thangaraju, B., Khalaf, O. I., Alotaibi, Y., & Alghamdi, S. (2021). Design and synthesis of multi-mode bandpass filter for wireless applications. *Electronics*, *10*(22), 2853. https://doi.org/10.3390/electronics10222853.

Palanisamy, S., Thangaraju, B., Khalaf, O. I., Alotaibi, Y., Alghamdi, S., & Alassery, F. (2021). A novel approach of design and analysis of a hexagonal fractal antenna array (HFAA) for next-generation wireless communication. *Energies*, *14*(19), 6204. https://doi.org/10.3390/en14196204.

Peng, L., Ruan, C. L., & Li, Z. Q. (2010). A novel compact and polarization-dependent mushroom-type EBG using CSRR for dual/triple-band applications. *IEEE Microwave and Wireless Components Letters*, *20*(9), 489-491.

Pham, Q. H., Ho, D., Khandaker, S., & Tran, A. T. (2022). Investigating the effects of Accounting Law on the Credit Rating Models using Artificial Neural Networks: a study in Vietnam. *Advances in Decision Sciences*, *26*(4), 1-32.

Prabhu, T., & Pandian, S. C. (2021). Design and development of planar antenna array for mimo application. *Wireless Networks*, *27*, 939-946.

Prabhu, T., Chenthur Pandian, S., & Suganya, E. (2021). Investigating the Performance of Planar Inverted-F Antenna (PIFA) in Dual Resonant Mode. In *2nd EAI International Conference on Big Data Innovation for Sustainable Cognitive Computing: BDCC 2019* (pp. 33-46). Springer International Publishing.

Prabhu, T., Pandian, S. C., & Suganya, E. (2019, March). Contact feeding techniques of rectangular microstrip patch antenna for 5 GHz Wi-Fi. In *2019 5th International conference on advanced computing & communication systems (ICACCS)* (pp. 1123-1127). IEEE.

Prabhu, T., Suganya, E., Ajayan, J., & Kumar, P. S. (2021). An intensive study of dual patch antennas with improved isolation for 5G mobile communication systems. In *Future Trends in 5G and 6G* (pp. 205-217). CRC Press.

Prabhu, T., Suganya, E., Ajayan, J., & Kumar, P. S. (2021). An intensive study of dual patch antennas with improved isolation for 5G mobile communication systems. In *Future Trends in 5G and 6G* (pp. 205-217). CRC Press.

Qamar, Z., Naeem, U., Khan, S. A., Chongcheawchamnan, M., & Shafique, M. F. (2016). Mutual coupling reduction for high-performance densely packed patch antenna arrays on finite substrate. *IEEE Transactions on Antennas and Propagation*, *64*(5), 1653-1660. doi: 1-1. 10.1109/TAP.2016.2535540.

Radisic, V., Qian, Y., Coccioli, R., & Itoh, T. (1998). Novel 2-D photonic bandgap structure for microstrip lines. *IEEE Microwave and guided wave letters*, *8*(2), 69-71.

Rafiei, V., Karamzadeh, S., & Saygin, H. (2018). Millimetre-wave high-gain circularly polarised SIW end-fire bow-tie antenna by utilising semi-planar helix unit cell. *Electronics Letters*, *54*(7), 411-412.

Ravinagarajan, J., & Sophia, S. (2022). Empirical Significance of Movements in Stock Trading Platforms in NSE Market Structure. *Advances in Decision Sciences*, *26*(3), 1-25.

Rifaee, M., Al Rawajbeh, M., AlOkosh, B., & Abdel-Fattah, F. (2022). A new approach to recognize human face under unconstrained environment. *Int. J. Advance Soft Compu. Appl*, *14*(2).

Tiku, M. L., Wong, W. K., Vaughan, D. C., & Bian, G. (2000). Time Series Models in Non-Normal Situations: Symmetric Innovations. *Journal of Time Series Analysis*, *21*(5), 571-596.

Satheesh Kumar, P., Jeevitha, & Manikandan. (2021). Diagnosing COVID-19 virus in the cardiovascular system using ANN. *Artificial Intelligence for COVID-19*, 63-75. https://doi.org/10.1007/978-3-030-69744-0_5.

Sharma, S. K., & Shafai, L. (2001, July). Enhanced performance of an aperture-coupled rectangular microstrip antenna on a simplified unipolar compact photonic band gap (UC-PBG) structure. In *IEEE Antennas and Propagation Society International Symposium. 2001 Digest. Held in conjunction with: USNC/URSI National Radio Science Meeting (Cat. No. 01CH37229)* (Vol. 2, pp. 498-501). IEEE.

Suganya, E., Prabhu, T., Palanisamy, S., Malik, P. K., Bilandi, N., & Gehlot, A. (2023). An Isolation Improvement for Closely Spaced MIMO Antenna Using λ/4 Distance for WLAN Applications. *International Journal of Antennas and Propagation*, *2023*. https://doi.org/10.1155/2023/4839134.

Suganyadevi, K., Nandhalal, V., Palanisamy, S., & Dhanasekaran, S. (2022, October). Data security and safety services using modified timed efficient stream loss-tolerant authentication in diverse models of VANET. In *2022 International Conference on Edge Computing and Applications (ICECAA)* (pp. 417-422). IEEE.

Tan, X., Wang, W., Wu, Y., Liu, Y., & Kishk, A. A. (2019). Enhancing isolation in dual-band meander-line multiple antenna by employing split EBG structure. *IEEE Transactions on Antennas and Propagation*, *67*(4), 2769-2774.

Wong, W. K., Yeung, D., & Lu, R. (2022). The mean-variance rule for investors with reverse S-shaped utility. *Annals of Financial Economics*, 2250030.

Xue, X., Chinnaperumal, S., Abdulsahib, G. M., Manyam, R. R., Marappan, R., Raju, S. K., & Khalaf, O. I. (2023). Design and Analysis of a Deep Learning Ensemble Framework Model for the Detection of COVID-19 and Pneumonia Using Large-Scale CT Scan and X-ray Image Datasets. *Bioengineering*, *10*(3), 363.

Xue, X., Marappan, R., Raju, S. K., Raghavan, R., Rajan, R., Khalaf, O. I., & Abdulsahib, G. M. (2023). Modelling and Analysis of Hybrid Transformation for Lossless Big Medical Image Compression. *Bioengineering*, *10*(3), 333.

Xue, X., Poonia, M., Abdulsahib, G. M., Bajaj, R. K., Khalaf, O. I., Dhumras, H., & Shukla, V. (2023). On Cohesive Fuzzy Sets, Operations and Properties with Applications in

Electromagnetic Signals and Solar Activities. *Symmetry*, *15*(3), 595. https://doi.org/10.3390/sym15030595.

Xue, X., Shanmugam, R., Palanisamy, S., Khalaf, O. I., Selvaraj, D., & Abdulsahib, G. M. (2023). A hybrid cross layer with harris-hawk-optimization-based efficient routing for wireless sensor networks. *Symmetry*, *15*(2), 438. https://doi.org/10.3390/sym15020438.

Yang, F., & Rahmat-Samii, Y. (2003). Microstrip antennas integrated with electromagnetic band-gap (EBG) structures: A low mutual coupling design for array applications. *IEEE transactions on antennas and propagation*, *51*(10), 2936-2946. doi: 10.1109/TAP.2003.817983.

Yang, W., Wang, H., Che, W., & Wang, J. (2013). A wideband and high-gain edge-fed patch antenna and array using artificial magnetic conductor structures. *IEEE Antennas and Wireless Propagation Letters*, *12*, 769-772. doi:10.1109/LAWP.2013.2270943.

Yang, X., Liu, Y., Xu, Y. X., & Gong, S. X. (2017). Isolation enhancement in patch antenna array with fractal UC-EBG structure and cross slot. *IEEE Antennas and Wireless Propagation Letters*, *16*, 2175-2178. doi: 10.1109/LAWP.2017.2703170.

Yasumoto, K. (Ed.). (2018). *Electromagnetic theory and applications for photonic crystals*. CRC press.